IEEE Access
Multidisciplinary | Rapid Review | Open Access Journal

Received 15 June 2022, accepted 26 June 2022, date of publication 6 July 2022, date of current version 15 July 2022.

Digital Object Identifier 10.1109/ACCESS.2022.3188760

RESEARCH ARTICLE

Adaptive Continuous Sliding Mode Control of Buck Converters With Multidisturbances Based on Zero-Crossing Detection

YANMIN WANG, (Member, IEEE), WEIQI ZHANG, AND CHEN XUE
School of Electrical Engineering and Automation, Harbin Institute of Technology, Harbin, Heilongjiang 150001, China
Corresponding author: Chen Xue (xuechen@stu.hit.edu.cn)

This work was supported in part by the National Natural Science Foundation of China under Grant 51307035 and Grant 62073095.

ABSTRACT In this paper, a novel adaptive continuous sliding mode (SM) control approach is proposed based on the robust stability analysis of buck converters with multi-disturbances. Instead of the traditional first-order SM methods, the twisting algorithm is adopted to realize the control continuity and further weaken their inherent chattering problem. By introducing the zero-crossing detection innovatively, the influence of the traditional twisting algorithm with fixed control gain led to the low precision is effectively eliminated, and the small region can be controlled due to the implementation of the adaptive time-varying control gain. In addition, the magnitude of the controller can be reduced to a minimal admissible level determined by the system stable conditions and the selection of optimization parameters. Furthermore, multiple model uncertainties and external disturbances are considered into the modeling of the buck converters and the proposed adaptive SM controllers to ensure the strong robustness of the whole system while suffering possible disturbances. Finally, comparative simulations and experiments are given to validate the effectiveness of the proposed adaptive control strategy.

INDEX TERMS Adaptive continuous sliding mode control, buck converters, zero-crossing detection, multi-disturbances, twisting sliding mode control.

I. INTRODUCTION

As a kind of power electronic equipment, buck converters have been widely used in many fields due to their simple topology, high efficiency and reliability [1], [2]. For the controlled buck converter, owing to the inclusion of nonlinear components such as the inductor, capacitor, and diode, which has different nonlinear static and dynamic characteristics in each operating mode, and is more susceptible to uncertainties and external disturbances and also presents certain challenges to the controllers [3], [4]. Meanwhile, the performances of most buck converters are not satisfactory under possible system parameter variations and external disturbances, this is since they are based on proportional integral derivative (PID) control methods, while PID controllers are not good at overcoming the adverse effects on system output precision control from the internal parameter variations of the system, sudden changes of the load or input power supply, interferences of the measurement device or external environment, and so on [5]–[7]. In order to obtain more satisfactory performances of buck converters, many researchers focus on the design of diverse kinds of auxiliary observers based on system descriptions and different types of controllers of buck converters [8]–[10].

For the auxiliary observers, the literature [11] presents a reduced-order-enhanced state observer-based control strategy for the buck converter against the disturbances. The literature [12] proposes the high-gain extended state observer, which effectively suppresses the detrimental effect of external noise on the buck system. The literature [13] introduces a single-loop disturbance observer-based control strategy of buck converters. Although auxiliary observers as an alternative solution are generally adopted to enhance the robustness and relieve the calculating burden of modeling buck converters for higher precision [14], [15], they increase the

The associate editor coordinating the review of this manuscript and approving it for publication was Mohammad Alshabi.

complexity of system analysis. Moreover, the single type of auxiliary observers cannot compensate for multi-possible model uncertainties and external disturbances simultaneously, and there are still many challenges in enhancing the output performances of buck converters under multiple disturbances.

The different types of controllers are related to the output performances of buck converters, which is concerned to be closely related to advanced nonlinear control strategies such as sliding mode control (SMC) [16]–[18], fuzzy control [19], [20], neural network [21], [22], and intelligent control [23], [24].

In much literature, SMC has been fully proved for its merits as strong robustness, easy implementation and good performance with the switching property, which can be well applied in controlling DC-DC converters [25]–[27]. For example, the linear sliding mode (LSM), terminal sliding mode control (TSMC), and non-singular terminal sliding mode control (NTSMC) methods for buck converters are proposed in [28], [29] and [30], respectively. In order to further enhance the ability of SMC to overcome model uncertainties and external disturbances, the control strategy combining SM controller and disturbance observers is proposed. In [31], an extended state observer is proposed based on SMC for buck converters subject to mismatched disturbances. In [32], the output voltage regulation problem of the boost converter system is addressed by using NTSMC based on the finite-time disturbance observer. And the literature [33] proposes a compound control method using an improved non-singular fast terminal sliding mode controller and the disturbance observer. Although the addition of the disturbance observers complements the SMC to some extent, which provides the possible control schemes for improving the response time and steady-state accuracy for the control of buck converters, this combination still suffers from two fatal drawbacks derived from traditional first-order SM (1-SM), i.e., the chattering phenomenon and the problem of unnecessary constant high control gain [34], [35].

The chattering problem of the traditional SM approaches will lead to high-frequency chattering occurring near the SM surface due to the switching of nonlinear control rate and inertia of the system [36], [37]. The problem can disrupt, damage, or wear the hardware circuits or even cause instability of buck converters. In order to eliminate the effects of chattering, the reaching control law [38], boundary layer [39], and fuzzy logic [40] are proposed respectively to realize the continuous approximation of switching control signals for suppressing the chattering of the system, however, above methods are at the price of performance degradation and the loss of robustness of the buck converters. Comparatively, the recently developed high-order sliding mode (HOSM) [41] is generally used for chattering suppression. Its idea is to design the switching control term sgn(·) originally placed on the first derivative of the sliding variables to act on their higher derivatives. Therefore the real control laws will be smoothed by the integral operation, and chattering elimination and the desired control continuity can be further obtained, and the second-order SM (2-SM) has developed as a popularly used type for the application in DC-DC converter systems [42], and the twisting algorithm [43], sub-optimal algorithm [44] and super-twisting algorithm [45] are among the most popular approaches. In order to enhance the output constraint of the 2-SM of the nonlinear system under disturbance, some researches also focus on the design scheme of the 2-SM based on the barrier Lyapunov function (BLF) [46]–[48]. Although the scheme of improving the 2-SM based on BLF has achieved some success in the anti-disturbance output constraint of the system, the complexity of BLF hinders the in-depth analysis of system stability, and the fixed control gains of 2-SM will still cause the low precision of buck converters when suffering from system parameter variations and external disturbances, which can be further investigated.

In order to solve the problem that the unnecessary control gain will lead to the low precision of buck converters when suffering possible disturbances under the traditional 2-SM control, the possible adaptive mechanism related to reducing the excessive control magnitude has arisen. Although some intelligent technologies such as fuzzy logic and neural network are combined with HOSM to adjust the system stability [49], [50], this combination is seldom applied in buck converters due to relying on the prior evaluation of experts. Therefore, some adaptive mechanisms based on Lyapunov stability and switch-time have been proposed as two typical alternative solutions. For the former, it can lead the control gain to decrease dynamically as the system converges to the equilibrium point and guarantee the stability of the system in the range of convergence [51], for example, the literature [52] proposes a novel adaptive intelligent global sliding mode control based on the Lyapunov stability theory to overcome the time-varying uncertainties of buck converters. In the literature [53], a Lyapunov-based adaptive-robust current controller is developed for DC-DC converters. The literature [54] proposed a Lyapunov-based nonlinear controller in the DC-DC converter to stabilize the system. However, the relationship between parameter adjustment and control performance of the system can hardly be obtained. For the latter, it inherits the characteristics of the ''switching'' of the traditional SMC and its adaptation mechanism relies on counting the number of zero-crossing of the sliding variable in a certain time interval [55], [56], it effectively deals with both state-dependent and time-varying control magnitude uncertainties by adjusting the control gain online based on judging whether the zero-crossings of the sliding variable meet the requirements [57]. However, the stability and control performance of the buck systems based on the switch-time method still need to be further investigated, and the adaptive magnitude of the controller can be further reduced.

Based on the above analysis, this paper proposes a novel adaptive twisting algorithm by introducing the zero-crossing checking mechanism to guarantee the control continuity and time-varying control gain of the buck converter concerning

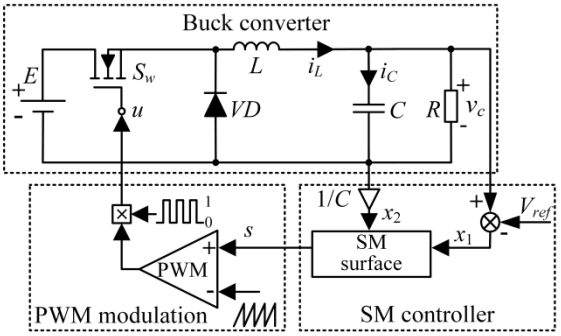

FIGURE 1. Diagram of buck control system with SMC.

multiple disturbances. To be specific, the major contributions of this paper can be concluded as follows:

1)The traditional twisting controller for the averaging state-space model describing buck converter is built, and the multiple model uncertainties and external disturbances are concerned. Further, the rigorous stability analysis on the phase plane is given by analyzing its characteristic phase trajectory.

2)A novel adaptive twisting algorithm based on the zero-crossing checking mechanism is proposed. The number of the zero-crossings can be calculated online for reducing the control gain to the minimum admissible level, and the system stability is investigated as an important issue.

3)The effectiveness and superiority of our proposed improved twisting algorithm, compared to the traditional SM, have been verified by simulation and experiment results.

This paper is organized as: Section II introduces the mathematical model of the buck converter with multi-disturbances. In Section III, the traditional twisting algorithm is designed for the comparison and the stability analysis is addressed respectively. Section IV includes the design of an improved adaptive twisting algorithm based on the zero-crossing checking mechanism, following its stability analysis is given. Furthermore, simulations and experiments are given in Section V to demonstrate the effectiveness of the novel proposed method. Finally, the conclusions of this paper are drawn in Section VI.

II. SYSTEM DESCRIPTION

Figure 1 gives the typical system diagram of the SM controlled DC/DC converter. In the converter circuit, E is the input DC voltage source with $0 < E < E_{max}$, where E_{max} is the maximum of E; v_c is the transient value of output voltage; VD is a current limiting diode; S_w is a power switch, which is often dominated by MOSFET and IGBT, and the pulse width modulation (PWM) technology is adopted for S_w to realize the duty ratio control, i.e., the duty ratio $u \in [0,1]$; L, C, and R represent an inductor, a capacitor, and a load resistor respectively; i_L and i_C are the currents flowing through the inductor and the capacitor respectively.

For the controlled buck converter in Fig.1, we assume it works in continuous conduction mode (CCM), i.e., the inductor current $i_L \neq 0$. Based on Kirchhoff's circuit law, and the model describing the ON/OFF operation of the buck converter can be expressed respectively as follow based on the approach of the average state-space modeling [5]

$$\begin{cases} \frac{di_L}{dt} = \frac{1}{L}(E - v_c) \\ \frac{dv_c}{dt} = \frac{1}{C}\left(i_L - \frac{v_c}{R}\right) \end{cases} \tag{1}$$

$$\begin{cases} \frac{di_L}{dt} = -\frac{1}{L}v_c \\ \frac{dv_c}{dt} = \frac{1}{C}\left(i_L - \frac{v_c}{R}\right) \end{cases} \tag{2}$$

By combining (1) and (2), it can yield

$$\begin{cases} \frac{di_L}{dt} = \frac{1}{L}(uE - v_c) \\ \frac{dv_c}{dt} = \frac{1}{C}\left(i_L - \frac{v_c}{R}\right) \end{cases} \tag{3}$$

By defining V_{ref} as the DC reference voltage of the output voltage v_c, and the state x_1 and x_2 are defined as the output voltage error and its derivative, here we assume that $\dot{V}_{ref} = 0$, and the output dynamic model of the system can be expressed as

$$\begin{cases} x_1 = v_c - V_{ref} \\ x_2 = \dot{x}_1 = \dot{v}_c - \dot{V}_{ref} = \dot{v}_c \end{cases} \tag{4}$$

A. MODELING THE BUCK CONVERTER UNDER DISTURBANCE

In this paper, we take the multiple model uncertainties and external disturbances into account in the system model (3). Based on (3), the variations of R, E, L, C and time-varying external disturbances $d_1(t)$ and $d_2(t)$ are introduced as follows

$$\begin{cases} \frac{di_L}{dt} = \frac{1}{L+\Delta L}\left[u(\Delta E + E) - v_c\right] + d_1(t) \\ \frac{dv_c}{dt} = \frac{1}{C+\Delta C}\left(i_L - \frac{v_c}{R+\Delta R}\right) + d_2(t) \end{cases} \tag{5}$$

where the terms with "Δ" are the corresponding disturbance variations of the nominal variables, the ΔR, ΔE, ΔL, and ΔC are the external and internal parameter disturbances of the system with their own assumption of the boundary $|\Delta R| \leq \psi_R < R$, $|\Delta E| \leq \psi_E < E$, $|\Delta L| \leq \psi_L < L$, $|\Delta C| \leq \psi_C < C$, where ψ_R, ψ_E, ψ_L and ψ_C are constants. Furthermore, $d_1(t)$, $d_2(t)$, and their derivatives with respect to time are also assumed to have their own boundaries with $|d_1(t)| \leq \psi_{d1}$, $|d_2(t)| \leq \psi_{d2}$, $|\dot{d}_1(t)| \leq \psi_{\dot{d}1}$ and $|\dot{d}_2(t)| \leq \psi_{\dot{d}2}$, where ψ_{d1}, ψ_{d2}, $\psi_{\dot{d}1}$ and $\psi_{\dot{d}2}$ are also constants.

Here we also define $|\Delta V_{ref}| \leq \psi_{Vref} < V_{ref}$ as the disturbance variation of the reference output voltage V_{ref} mentioned in (4) with the boundary constant ψ_{Vref}, which can be considered as another external disturbance of the system. Combining (4) and (5) by taking the above multiple disturbances into account, the dynamic equation can yield as

$$\begin{cases} \dot{x}_1 = x_2 \\ \dot{x}_2 = D_1 x_1 + D_2 x_2 + D_3 u + D_4(t) \end{cases} \tag{6}$$

with

$$D_1 = \frac{-1}{(C+\Delta C)(L+\Delta L)} \tag{7}$$

$$D_2 = \frac{-1}{(C+\Delta C)(R+\Delta R)} \tag{8}$$

$$D_3 = \frac{E+\Delta E}{(C+\Delta C)(L+\Delta L)} \tag{9}$$

$$D_4(t) = \frac{d_1(t)}{C+\Delta C} + \dot{d}_2(t) - \frac{V_{ref}+\Delta V_{ref}}{(C+\Delta C)(L+\Delta L)} \tag{10}$$

It should be noted that multiple disturbances of the buck converter system are considered in (5) with their own boundary limitations. Therefore, the $\psi_{D1} \le D_1 < 0$, $\psi_{D2} \le D_2 < 0$, $0 < D_3 \le \psi_{D3}$ can be obtained from (7)-(9), and $|D_4(t)| \le \psi_{D4}$ can also be derived from (10), where ψ_{D1}, ψ_{D2}, ψ_{D3} and ψ_{D4} are boundary constants.

B. DESCRIPTION OF THE SM CONTROLLER

In the design of SM controllers applied in DC-DC converters, the first- and second-order SM control methods are mainly used at present [58], [59]. The controller design usually consists of a sliding surface and a continuous or discontinuous control law design. Therefore, for the buck converter system in (6), a linear sliding surface and the commonly used discontinuous control law can be designed as follows [28]

$$s = c_1 x_1 + x_2 \tag{11}$$

$$u = -\frac{1}{2}[sgn(s) - 1] \tag{12}$$

where the design parameters $c_1 > 0$, x_1 and x_2 can be obtained directly by measuring the voltage v_c and current i_L of the system by using the hall sensors, which are simple and easy to implement. Once the system states are forced to and maintained on the sliding mode surface $s = 0$ in (11) by the control law u in (12), its dynamic and static performances will be absolutely determined by the first-order differential equation $\dot{x}_1 = -c_1 x_1$, i.e., the derivative of the output voltage error $x_1 = x_1(0)e^{-c_1 t}$ converges exponentially to the equilibrium origin, where $x_1(0)$ is the initial value of the state x_1. Obviously, the greater the c_1 is, the faster the system converges.

In terms of control laws, the design of both first and second-order SM needs to meet the sliding mode arrival condition to ensure the system stability. However, from the mechanism of HOSM chattering suppression based on relative order [41]–[45], the difference between the two is that: the 1-SM will switch the control term sgn(·) acting on the $\dot{s}$ to ensure the existence of $s = 0$ [28]–[30]. Then the system states continue to converge, and finally $x_1 = x_2 = 0$ can be realized according to (11), but the chattering problem still exists. For the 2-SM, as the simplest HOSM, the term sgn(·) is designed to act on $\ddot{s}$, which means that the sgn(·) suffers the action of the first field integral or low-pass filtering, so that the actual control law is converted to be continuous. And the convergence of the 2-SM $s = \dot{s} = 0$ and the system state $x_1 = x_2 = 0$ are realized simultaneously.

III. TRADITIONAL FIXED GAIN SECOND-ORDER SMC ALGORITHM

In this section, we take the commonly used Twisting algorithm to elaborate the chattering suppression mechanism of the 2-SM algorithm in detail, which lays the foundation for the propose of the adaptive continuous SMC of buck system based on zero-crossing detection and performance comparisons in this paper.

A. DESIGN OF TRADITIONAL TWISTING CONTROLLER

For the buck converter with actual voltage regulating capacity, the sliding surface of the traditional twisting algorithm is also selected in the linear form in (11). To guarantee the system converges to the sliding surface s, the derivative of the control law can be generally designed as

$$\dot{u} = -r_1 sgn(s) - r_2 sgn(\dot{s}) \tag{13}$$

where, the control gain $r_1 > r_2 > 0$, and the range of r_1 and r_2 are related to the response speed and steady-state error of the system [41]. Due to the switching control term sgn(·) is located on the first-order derivative of the control law u in (13), which makes the real u continuous through integration. In other words, the control continuity can be achieved and the first- and second-order sliding variable $s = \dot{s} = 0$ can be guaranteed, it is why the twisting algorithm can effectively weaken the chattering problem in SMC.

Combining with (6) and (11), the second-order derivative of sliding variable s with respect to time can be calculated, the corresponding switching term sgn(·) can also be got directly, and there is

$$\ddot{s} = h(x_1, x_2, u, t) + D_3 \dot{u} \tag{14}$$

with

$$h(x_1, x_2, u, t) = D_1(c_1 + D_2)x_1 + [D_1 + D_2(c_1 + D_2)]x_2 + D_3(c_1 + D_2)u + \dot{D}_4(t) \tag{15}$$

From (14), we can see that the derivative $\dot{u}$ appears directly in the second-order derivative $\ddot{s}$. And the range of D_3 will affect the amplitude variation of u and limit the stability conditions of the system. Therefore, the range of D_3 will further be constrained as $\mu_{\min} \le D_3 \le \mu_{\max}$, where $\mu_{\min} > 0$ and $\mu_{\max} \le \psi_{D3}$. And for $h(x_1, x_2, u, t)$, because of the duty ratio $u \in [0,1]$, the function $h(x_1, x_2, u, t)$ is bounded with

$$\sup |h(x_1, x_2, u, t)| \le H \tag{16}$$

considering $\mu_{\min} \le D_3 \le \mu_{\max}$ and (16) together, it follows that $\ddot{s}$ is bounded.

B. THE ANALYSIS OF THE TWISTING ALGORITHM CONTROL SYSTEM STABILITY

Theorem 1: For the buck converter in (6), if the sliding surface s and control law u are respectively designed as (11) and (13), and the finite-time stability condition of the twisting

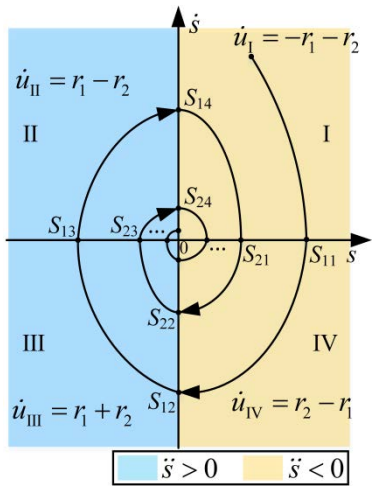

FIGURE 2. Convergence trajectory of the buck converter with twisting algorithm.

algorithm control system concerning the design parameters r_1 and r_2 can be deduced as

$$\begin{cases} \mu_{\min}(r_1 + r_2) - H > \mu_{\max}(r_1 - r_2) + H \\ \mu_{\min}(r_1 - r_2) - H > 0 \end{cases} \tag{17}$$

Proof: From (14) to (16), we can get the limitation of $\ddot{s}$ as

$$\ddot{s} \in [-H, H] + [\mu_{\min}, \mu_{\max}]\dot{u} \tag{18}$$

Considering the stability condition of HOSM [41] and (18), whether the system under the twisting algorithm can remain stable is closely related to the states of the $\dot{u}$ and $\ddot{s}$. And as its name suggests, the sliding variable s will converge to the equilibrium origin in a spiral trajectory in the phase plane $s - \dot{s}$, which can be seen in Figure 2. And the $\dot{u}$ and $\ddot{s}$ will show different states with the time-varying variable s, which can be divided into four quadrants I to IV in Fig.2.

For the convenience of marking the intersections of the spiral trajectory and the axis in the phase plane $s-\dot{s}$, the point set $\{S_{ij}|i = 1, 2, 3, \ldots; j = 1, 2, 3, \ldots\}$ can be used to describe all the intersections. As shown in Fig.2, with the system states converging to the equilibrium point, the spiral trajectory of s indents inwards, causing the radius of the spiral trajectory decreases with each turn. And there should be $|S_{ij}| > |S_{(i+1)j}|$ and $|S_{ij}| > |S_{i(j+1)}|$ to ensure that the trajectory radius of the $(i+1)$-th turn is less than the i-th turn always.

Based on the characteristics of the trajectory of the twisting algorithm control system, here we take the trajectory of $S_{12} \rightarrow S_{22}$ as an example, and the sign of the $\ddot{s}$ can be investigated in two cases: $\ddot{s} \geq 0$ and $\ddot{s} < 0$ in $s-\dot{s}$ respectively shown in Fig.2.

Case 1: In Fig.2, When the system states are located in the quadrant III of $\ddot{s} \geq 0$ and converge along with $S_{12} \rightarrow S_{14}$, the $\dot{s}$ will change from negative to positive. And the $\ddot{s}$ also changes over time with $\dot{u}_{III} = r_1 + r_2$ from (14) and (15). While the $\dot{u}$ in quadrant II becomes $\dot{u}_{II} = r_1 - r_2$ after the time-varying $\ddot{s}$ crossing the spinodal S_{13}, which still remains $\dot{u} > 0$ due to $r_1 > r_2 > 0$ in (12), but $\dot{u}_{II} < \dot{u}_{III}$, and then the states will cross S_{14} with the increasing u and enter the area of $\ddot{s} < 0$, and there is $|S_{12}| < |S_{14}|$ in Fig.2. In order to ensure that the system states converge along the twisting trajectory and remain stable, the following relationship must be guaranteed in the whole process of converging as

$$\begin{cases} \ddot{s}_{III\,\min} > \ddot{s}_{II\,\max} \\ \ddot{s}_{II\,\min} > 0 \end{cases} \tag{19}$$

where $\ddot{s}_{II}$ and $\ddot{s}_{III}$ are the value of $\ddot{s}$ in areas II and III respectively. Further substituting (14)-(16) into (19), then the stability condition in (17) can be deduced.

Case 2: Since the $\dot{u}$ is symmetric in quadrants I, III and II, IV, when the system states are located in the quadrant I of $\ddot{s} < 0$ and converge along $S_{14} \rightarrow S_{22}$, the $\dot{s}$ will change from positive to negative, and with the decreasing u in IV, the state will cross the spinodal S_{22} and return to the area of $\ddot{s} \geq 0$. Similar to the analysis with (19), the following relationship must be guaranteed in the whole process of converging as

$$\begin{cases} \ddot{s}_{I\,\min} < \ddot{s}_{IV\,\max} \\ \ddot{s}_{IV\,\min} < 0 \end{cases} \tag{20}$$

where $\ddot{s}_I$ and $\ddot{s}_{IV}$ are the value of $\ddot{s}$ in areas I and IV respectively. Further substituting (14)-(16) into (20), the system stability condition in (17) can also be deduced.

Remark 1: It should be noted that, the control gains r_1 and r_2 in (12) and (17) of the traditional twisting algorithm are fixed, which are generally determined by the prior evaluation of experts and are not suitable for the time-varying convergence characteristics of the system with disturbances, i.e., when system gradually approaching to the equilibrium origin or suffering disturbances, the unnecessary large control magnitude will damage the output accuracy and steady-state performance of the system, or the deficient small control magnitude will slow the response time of the system.

IV. IMPROVED ADAPTIVE TWISTING ALGORITHM FOR BUCK CONVERTERS

In order to solve the above problem of the unnecessary constant control gains for the traditional twisting algorithm, in this paper, an improved adaptive twisting algorithm based on the adaptive mechanism of online zero-crossing detection is proposed in the following. The design of the controller includes two parts: an improved sliding surface and a continuous control law.

A. IMPROVEMENT AND ANALYSIS OF SLIDING SURFACE

In order to improve the steady-state performance of the buck converter, different from the traditional sliding surface in (11), the integral term of the system state with x_1 is purposefully introduced as follows

$$s = c_1 x_1 + x_2 + c_2 \int_0^t x_1 dt \tag{21}$$

where the parameters $c_1 > 0$ and $c_2 > 0$. And the introduction of the integral term is to decrease the steady error of the

output voltage of the multi-disturbed system in (6). It should be noted that, in the integral term added, a bigger c_2 can get the smaller steady error of the buck system but at the price of less slow speed while the system states converging.

Considering the subsequent design of the control laws and stability analysis with the existence of $s = \dot{s} = 0$ of the twisting algorithm base on the online zero-crossing detection, the first and second-order derivatives of s with respect to time should be further obtained and the boundary of related parameters in the expression of $\ddot{s}$ should be determined, just like (18) in the traditional twisting algorithm.

In order to facilitate the subsequent expression of the second-order derivative of s, here we can define a new vector $\boldsymbol{w} = [w_1, w_2]^T = [\int_0^t x_1 dt, x_1]^T$, by combining with (6), the (21) can be rewritten as

$$\begin{cases} \dot{w}_1 = w_2 \\ \dot{w}_2 = -c_1 w_2 - c_2 w_1 + s \end{cases} \tag{22}$$

Substituting (22) to the first-order derivative of (21), and the $\dot{s}$ can be expressed as

$$\dot{s} = y_1 + \mu u \tag{23}$$

with

$$\begin{aligned} y_1 = {} & (c_1 + D_2)\, s + (-c_1 c_2 - c_2 D_4)\, w_1 \\ & + \left(-c_1^2 - c_1 D_2 + c_2 + D_1\right) w_2 + D_4\,(t) \end{aligned} \tag{24}$$

As mentioned in (14), the switch control term sgn(·) will further appear in the expression of $\ddot{s}$, which can be described from (23) as

$$\ddot{s} = y_{21}\,(\boldsymbol{w}, s) + y_{22}\,(u) + y_{23}\,(t) + D_3 \dot{u} \tag{25}$$

with

$$\begin{aligned} y_{21}\,(\boldsymbol{w}, s) = {} & \left(c_1 c_2 \beta_2 + c_2 \beta_1 - c_2 \beta_2^2 - c_2^2\right) \boldsymbol{w}_1 \\ & + \left(\beta_1 \beta_2 - c_1 c_2 + c_1^2 \beta_2 - c_1 \beta_2^2\right) \boldsymbol{w}_2 \\ & + \left(c_2 - \beta_1 - c_1 \beta_2 + \beta_2^2\right) \boldsymbol{s} \end{aligned} \tag{26}$$

$$y_{22}\,(u) = (c_1 - \beta_2)\, D_3 u \tag{27}$$

$$y_{23}\,(t) = (c_1 - \beta_2)\, \beta_3 + \dot{\beta}_3 \tag{28}$$

where $\beta_1 = -D_1 > 0$, $\beta_2 = -D_2 > 0$, $\beta_3(t) = |D_4(t)| > 0$.

In order to further elaborate the boundary of the parameters in (25)-(28) relating with $\ddot{s}$ conveniently, here the constants $\zeta_1, \zeta_2, \zeta_3$ and the functions $\zeta_4(t)$, $Y_{21}(||\boldsymbol{w}||, |s|)$, $Y_{22}(u)$, $Y_{23}(t)$ are defined from (25)-(28) as

$$\begin{cases} \zeta_1 = \max\{c_1, \beta_2\} \\ \zeta_2 = \max\left\{\left|c_1 c_2 \beta_2 + c_2 \beta_1 - c_2 \beta_2^2 - c_1^2\right|, \right. \\ \left. \left|\beta_1 \beta_2 + c_1^2 \beta_2 - c_1 \beta_2^2 - c_1 c_2\right|\right\} \\ \zeta_3 = \max\left\{\left|c_1 \beta_2 + \beta_1\right|, \left|c_2 + \beta_2^2\right|\right\} \\ \zeta_4\,(t) = \max\left\{\beta_3\,(t), \dot{\beta}_3\,(t)\right\} \end{cases} \tag{29}$$

$$\begin{cases} Y_{21}\,(\|\boldsymbol{w}\|, |s|) = \zeta_2\,(|w_1| + |w_2|) + \zeta_3\,|s| \\ Y_{22}\,(u) = \zeta_1 D_3 u \\ Y_{23}\,(t) = \zeta_1 \zeta_4\,(t) \end{cases} \tag{30}$$

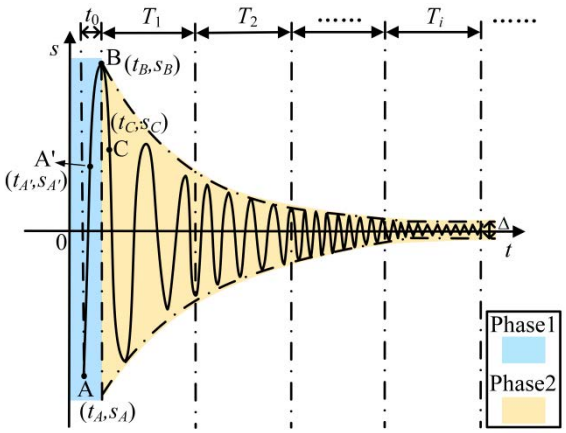

FIGURE 3. Convergence progress of adaptive control systems.

By comparing (26), (27), and (28) with (30), we can get the boundary condition of the terms in (25) as follow

$$\begin{cases} |y_{21}\,(\boldsymbol{w}, s)| \le Y_{21}\,(\|\boldsymbol{w}\|, |s|) \\ |y_{22}\,(u)| \le Y_{22}\,(u) \\ |y_{23}\,(t)| \le Y_{23}\,(t) \end{cases} \tag{31}$$

B. IMPROVEMENT OF THE ADAPTIVE CONTROL LAW WITH STABILITY ANALYSIS

In the design of the control law u, based on the principle of switching time [57], the whole convergence process of the system can be divided into two phases, as shown in Figure 3.

The first phase is from the initial point A to the point B, which is the first peak point satisfying $\dot{s} = 0$ of the trajectory; and the second stage is after the point B, which can be divided into the equal time intervals with the sampling time T for counting the zero-crossings and can be represented as $\{T_1, T_2, \ldots T_i\}$. In particular, the expected steady-state error Δ is incorporated into the improvement of the traditional twisting control law in (13). And the control law u is decomposed into u_1 and u_2 corresponding to the two phases.

(1)Phase 1: (Point A-Point B): It starts from the initial Point A(t_A, s_A) and ends at Point B(t_B, s_B) which is satisfied with $\dot{s}(t_B) = 0$. In this phase, it is necessary to guarantee the buck system in (6) can complete the process from point A to point B within the finite $t_0\,(t_0 = t_B - t_A)$, so as to ensure that the subsequent adaptive converge can be carried out effectively. In order to meet the condition $\dot{s}(t_B) = 0$, the initialized control law u_1 can be further designed as following

$$\dot{u}_1 = -U\,(\boldsymbol{w}, s, u_1, t)\, sgn\,(s) \tag{32}$$

with

$$\begin{aligned} & U\,(\boldsymbol{w}, s, u_1, t) \\ & = \frac{1}{\mu_{\min}} Y \\ & = \frac{1}{\mu_{\min}} \left[Y_{21}\,(\|\boldsymbol{w}\|, |s|) + Y_{22}\,(|u_1|) + Y_{23}\,(t) + k\right] \\ & = \frac{1}{\mu_{\min}} \left[\zeta_2\,(|w_1| + |w_2|) + \zeta_3\,|s| + \zeta_1 D_3\,|u_1|\right. \end{aligned}$$

$$+\zeta_1\zeta_4(t)+k] \tag{33}$$

where the design parameter $k > 0$; $\mu_{\min}$ and $\mu_{\max}$ are the maximum and minimum of D_3 in (14). The constant Y is designed for setting the parameters of the adaptive control law u_2 to be applied in the successive time interval in phase 2. And the procedure of computing the constant Y, which is based on certain measurements to be taken online at $t = t_B$.

Theorem 2: For the buck converter in (6), the sliding surface is designed as (21) and the control law in phase 1 is designed as (32) and (33), then there must be a time t_B making $\dot{s}(t_B) = 0$ only if the sliding variable s is satisfied with $sgn(s)\cdot\ddot{s} \le -k$ or $s\cdot\ddot{s} \le -k|s|$.

Proof: The proof of Theorem 2 is divided into two steps.

Step 1: First is the proof of the existence of $sgn(s)\cdot\ddot{s} \le -k$ or $s\cdot\ddot{s} \le -k|s|$ in the control process.

By substituting (30), (32), and (33) into (25), it can be rewritten as follows

$$\begin{aligned}\ddot{s} &= y_{21}(\boldsymbol{w}, s) + y_{22}(u) + y_{23}(t) + D_3\dot{u}\\ &= y_{21} + y_{22} + y_{23} - D_3 sgn(s)\frac{1}{\mu_{\min}}[\zeta_2(|w_1|\\ &\quad + |w_2|) + \zeta_3|s|\\ &\quad +\zeta_2\mu|u_1| + \zeta_1\zeta_4(t) + k]\\ &= y_{21} + y_{22} + y_{23} - \frac{D_3}{\mu_{\min}}[Y_{21} + Y_{22} + Y_{23} + k]\,sgn(s)\end{aligned} \tag{34}$$

Then by combining (31) and (34), it can be obtained that

$$\begin{aligned}sgn(s)\ddot{s} &= sgn(s)[y_{21} + y_{22} + y_{23}\\ &\quad -\frac{D_3}{\mu_{\min}}(Y_{21} + Y_{22} + Y_{23} + k)\Big]\\ &\le sgn(s)[y_{21} + y_{22} + y_{23}]\\ &\quad -|y_{21}| - |y_{22}| - |y_{23}| - k\\ &\le |y_{21}| + |y_{22}| + |y_{23}| - |y_{21}| - |y_{22}| - |y_{23}| - k\\ &\le -k < 0\end{aligned} \tag{35}$$

and the $sgn(s)\cdot\ddot{s} \le -k$ can be seen from (35) easily, by multiplying both sides of $sgn(s)\cdot\ddot{s} \le -k$ by the term $|s|$ and then $s\cdot\ddot{s} \le -k|s|$ can be further obtained.

Step 2: This step is to prove the existence of $\dot{s}(t_B) = 0$ while the condition in Theorem 1 is satisfied.

Giving the initial state $(s(t_A), \dot{s}(t_A))$ of the system in Fig.3, considering their values of positive or negative as following cases:

Case 1: When $\dot{s}(t_A) > 0$, $s(t_A) > 0$, according to (35), $\ddot{s}(t_A) < 0$, causing the $\dot{s}$ monotonicity decreases, there will be $\dot{s}(t_A) < 0$ when a certain moment $t_C > t_A$, where t_C is the moment when the system state reaches a certain point C after passing through point B in Fig.3, and it means that the $\dot{s}(t_B) = 0$ will be satisfied with a certain moment $t_A < t_B < t_C$;

Case 2: When $\dot{s}(t_A) > 0$, $s(t_A) < 0$, $\ddot{s}(t_A) > 0$ can be seen from (35), casing the s and $\dot{s}$ monotonicity increases respectively, then there will be $s(t_{A'}) > 0$ when $t_C > t_{A'}$, where A' is another initial state different from A in Fig.3. And

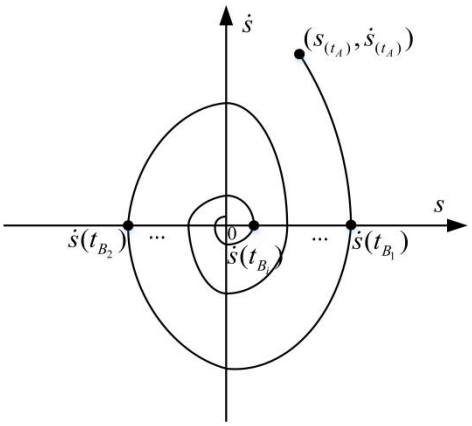

FIGURE 4. Diagram of phase trajectory of $\dot{s}$ crossing zero.

then it will repete the condition likes case 1, i.e., the $\dot{s}(t_B) = 0$ will be satisfied with a certain moment $t_{A'} < t_B < t_C$;

Case 3: When $\dot{s}(t_A) < 0$, $s(t_A) < 0$, it is the exact opposite of the situation in case 1, and there also will be $\dot{s}(t_B) = 0$ with a certain moment $t_A < t_B < t_C$;

Case 4: When $\dot{s}(t_A) < 0$, $s(t_A) > 0$, it is the opposite of case 2, and the existence of $\dot{s}(t_B) = 0$ can also be proved at the moment $t_{A'} < t_B < t_C$.

The four cases above can be represented by the twisting curve in Figure 4, which shows that for the arbitrary initial state $(s(t_A), \dot{s}(t_A))$, it will eventually arrive at the $\dot{s}(t_{B_i}))(i = 1,2,3\ldots)$ corresponding to each zero. So far the Theorem 2 has been proved.

(2)Phase 2: It refers to the convergence process after Point B or $t > t_B$. In this phase, the adaptive mechanism based on the zero-crossing checking will be carried out.

To improve the output performance of the buck system with arbitrarily small control accuracy within the range of convergence, Δ is denoted as the expected steady-state error of sliding variable s in Fig.3. Then the adaptive control law u_2 with the capability of online magnitude adjustment will be given as follow by comparing with (13)

$$\dot{u}_2 = -U_i[sgn(s) + r_4 sgn(\dot{s})] \tag{36}$$

where the design parameter $r_4 > 0$, and U_i is the continuously changing adaptive adjustment control gain by checking the number of zeros crossed by s in the time interval T_i in Fig.3, which can be expressed as

$$U_{i+1} = \begin{cases}\max(U_i - \Lambda_1 T, 0) & N_i \ge N^*\\ \min(U_i + \Lambda_2 T, U_0) & N_i < N^*\end{cases} \tag{37}$$

where N_i is the number of zero-crossing of s in the time interval T_i; N^* is the given reference number of zero-crossings with $N^* \ge 2$; Λ_1 and Λ_2 are positive constants with $\Lambda_1 < \Lambda_2$; U_0 is the initial value of u_2 at Point B and also chosen as the maximum value of $U(\boldsymbol{w}, s, u_1, t)$ at Point B of Phase 1 in (33) as

$$U_0 = \left[Y_{21}\left(\|\boldsymbol{w}\|^*, |s(t_B)|\right) + Y_{22}(u_{1\max}) + Y_{23}(t_B) + k\right] \tag{38}$$

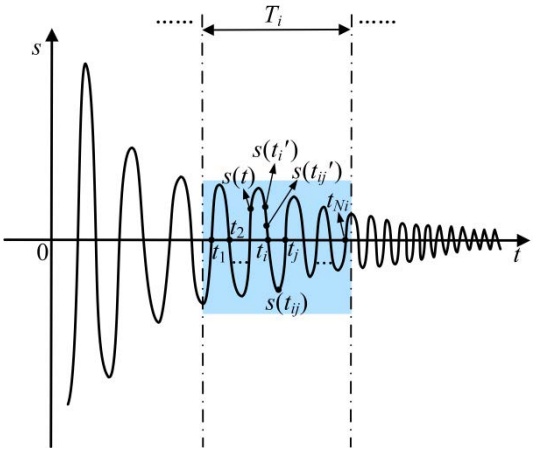

FIGURE 5. The process of online zero-crossing checking.

where $u_{1\max}$ is the maximum value of the control u_1 defined in (32) and the definition of $||\boldsymbol{w}||^*$ can be described as

$$\|\boldsymbol{w}\|^* = [w_1(x_1(t_B)), w_2(x_1(t_B))] + \boldsymbol{q} \tag{39}$$

where $\boldsymbol{q}$=[q_1, q_2], q_1 and q_2 are parameters satisfying $q_1 > 0$, $q_1 > 0$.

Theorem 3: For the dynamic system (6) in phase 2, if the improved sliding mode surface is designed as (21) and the adaptive control law is designed as (36)-(37), then the sliding variable s and its derivative $\dot{s}$ of the system can be guaranteed to converge to the range as

$$|\dot{s}| \le [U_0 + (1 + r_4)\,\mu_{\max} U_i]\,T \tag{40}$$

$$|s| \le [U_0 + (1 + r_4)\,\mu_{\max} U_i]\,T^2 \tag{41}$$

Proof: When the buck converter working under the adaptive controller in phase 2, by substituting the u_2 with variable amplitude in (36)-(37) into (25), we can get

$$\begin{aligned}\ddot{s} &= y_{21} + y_{22} + y_{23} + D_3\{-U_i[sgn(s) + r_4 sgn(\dot{s})]\} \\ &\le |y_{21}| + |y_{22}| + |y_{23}| + (1 + r_4)\,D_3 U_i\end{aligned} \tag{42}$$

As shown in Fig.3, the point B is the location of the first peak in phase 1 and also the maximum amplitude of oscillation in phase 2. Therefore, by combining (30), (31), and (38), (39), then (42) can be further changed into

$$\begin{aligned}\ddot{s} &\le Y_{21}[\|\boldsymbol{w}\|*, |s(t_B)|] + Y_{22}(u_{1\max}) + Y_{23}(t_B) + k \\ &\quad +(1 + r_4)D_3 U_i \\ &\le U_0 + (1 + r_4)\mu_{\max} U_i\end{aligned} \tag{43}$$

Here, we take the sampling interval T_i as an example to give the analysis of the zero-crossing of system states and further examine the range of $\ddot{s}$ within a single sampling interval T. As shown in Figure 5, we assume that there are any two zero-crossings ($s(t_i) = 0$ and $s(t_j) = 0$) at the moment t_i and t_j in T, where $i, j \in [1, N_i]$, and the N_i is the i-th zero-crossing in the sampling interval T_i. Because of the reference number of zero-crossings giving value $N^* \ge 2$, which means that at least twice zero-crossings occur within a single sampling interval T. Therefore, according to Rolle's theorem, there must be a state as $\dot{s}(t_{ij}) = 0$ when $t_i < t_{ij} < t_j$, which has been illustrated in Fig.5. After getting the state $\dot{s}(t_{ij})$, based on the Lagrange mean value theorem, we can further find another state $\dot{s}(t_{ij}')$ at the moment t_{ij}' between t and t_{ij} shown in Fig.5, and the state $\dot{s}(t_{ij}')$ will satisfy the following constraints according to (43)

$$\left|\ddot{s}\left(t_{ij}'\right)\right| = \left|\frac{\dot{s}(t) - \dot{s}\left(t_{ij}\right)}{t - t_{ij}}\right| \le [U_0 + (1 + r_4)\,\mu_{\max} U_i] \tag{44}$$

where t is any time except t_{ij} in the sampling interval of T_i, and satisfies $|t - t_{ij}| < T$.

Similar to (44), there also must exist another moment t_i' between t and t_i in Fig.5 and satisfying

$$\begin{aligned}\left|s\left(t_i'\right)\right| &= \left|\frac{\dot{s}(t) - \dot{s}\left(t'\right)}{t - t_i}\right| \\ &\le \left[U_0 + (1 + r_4)\,\mu_{\max} U_j\right]|t - t_i| \\ &\le \left[U_0 + (1 + r_4)\,\mu_{\max} U_j\right]T\end{aligned} \tag{45}$$

where t is also any time except t_i in T_i, and satisfies $|t - t_i| < T$. Then the range of $\dot{s}$ in (40) is proved. And the convergence range of s in (41) can be further deduced by simple time-integration of (45). The system's convergence has been proved by Theorem 1. So far, Theorem 3 has been proved.

Remark 2: As can be seen from Fig.3, as time changes, the smaller the oscillation amplitude of the sliding variable s is, while the bigger the number of zero-crossing N_i will be. According to (37) and (41), the relationship between N_i and N^* determines the adjustment range of U_i in the next detection cycle and the convergence effect of in this whole phase, and further indirectly controls the steady-state performance of the system. Therefore, the selection of N^* is crucial, which determines the steady-state error $s \le \Delta$ and further affects the desirable output accuracy of the system. In real buck converters, the N^* is usually determined by experiment with $N^* = \max\{2\,Tf_i + 1\}$(i= 1,2,3,...), where T is the time width and f_i is the zero-crossing oscillation frequency of s measured in time interval T_i, and $f_i = N_i/T$.

Remark 3: Equations (40) and (41) give the minimum range in which the system state can be stable in a finite time when the parameters are given. Furthermore, it can be seen from (41) that the minimum stability range of s is closely related to the value U_0 of the first peak point B in (40), and for guaranteeing that the limitation in (40) and (41), the single sampling interval T of the adaptive zero-crossing detection mechanism should meet the following conditions:

$$T < \frac{\sqrt{|s(t_B)| + \|\boldsymbol{q}\|}}{U_0 + (1 + r_4)\,\mu_{\max} U_i} \tag{46}$$

where s_B is the sliding variable value of Point B in Fig.3, the $\boldsymbol{q}$ is the vector in (39), and the arbitrary positive parameters q_1 and q_2 in $\boldsymbol{q}$ allow us to enlarge the admissible range for T as desired, which can help to adjust the amplitude of the controller more accurately online.

TABLE 1. Circuit parameters of buck converter.

Symbol	Quantity	Values
L	inductance	1mH
C	capacitance	1000μF
R	load resistance	10Ω
V_{ref}	the reference voltage	5V
E	input DC voltage	10V

TABLE 2. Comparison of voltage and current in rated working case.

SMC Algorithm	Output Voltage v_c		Inductor Current i_L	
	Steady-State Error(mV)	Converge-nce Time(s)	Steady-State Error(A)	Converge-nce Time(s)
1-SMC	15.13	0.055	0.098	0.057
2T-SMC	6.09	0.042	0.113	0.043
2AT-SMC	3.01	0.031	0.101	0.032

V. SIMULATIONS AND EXPERIMENTS

For the buck converter shown in Fig.1, the circuit parameters are listed in Table 1. In order to verify the superiority of the proposed adaptive continuous SMC based on the zero-crossing detection in terms of chattering suppression, response speed, and control accuracy, the performance was compared with the 1-SM represented by LSM in [28] and the 2-SM represented by the traditional twisting algorithm. The traditional LSM could be generally designed as (11) and (12).

In the following, for the convenience of introduction, the LSM, the traditional twisting algorithm, and the improved twisting algorithm are abbreviated as "1-SMC", "2T-SMC" and "2AT-SMC" respectively.

A. SIMULATIONS RESULTS AND ANALYSIS

For the traditional twisting algorithm in (11) and (13), the controller parameters are chosen as $c_1 = 110$, $r_1 = 320$, $r_2 = 300$; for the improved twisting algorithm in (21), (32)-(33) and (36)-(38), the parameters of the controller are designed as $c_2 = 0.1$, $k = 45$, $\Lambda_1 = 12$, $\Lambda_2 = 24$, $N^* = 8$, $T = 40\ \mu$s. As for the traditional LSM, the parameter of the sliding surface is also designed as $c_1 = 110$ for comparison. In order to satisfy the ON/OFF control of the power switch S_w in the buck converter, the PWM technology is adopted in the simulations as shown in Fig.1.

As the buck converter in (6) considers multiple internal and external disturbances of the system, in order to more intuitively see the performance comparisons of the above three methods, the buck system with rated or poor working conditions are considered in the following simulations, which are presented as: undisturbed and multi-disturbed.

Case 1: Rated working condition without any disturbances.

The comparisons of control performance between the three methods under rated working conditions are shown in Figure 6 and Table 2.

The Figure 6(a) and (b) shows the simulation results of output voltage v_c and inductance current i_L, respectively, it can be observed that the three SMC algorithms all can achieve constraint control of both of v_c and i_L. When the output voltage v_c converges to the given value $V_{ref} = 5$V, wherein the steady-state error of 1-SMC is 15.13mV, followed by that of 2T-SMC, which is 6.09mV, and 2AT-SMC has the best steady-state performance, which is only 3.01mV [61]. The chattering attenuation performance of 2AT-SMC is attributed to the introduction of the integral term of system state into the design of the sliding mode surface in this paper. And in addition to this, the system dynamic response speed under 2AT-SMC control is also the fastest, which is only about 0.031s, considering together with the control law u shown in Fig.6(c), which can be attributed to the variable gain control effect of the improved 2AT-SMC algorithm. Further, in Fig.6(d), we can see that the sliding variable s of 2AT-SM converges rapidly in 0.01s, but compared with 2T-SM, due to the limitation of its fixed gain, the convergence speed of s is relatively slow, reaching steady-state only at 0.034s, and the state s fluctuates within a certain range, which cannot meet the requirements of high output accuracy of the buck converter.

And it can be seen from Fig.6(d) that the oscillation of the initial trajectory of s is the largest in the beginning corresponding to the phase 1 in Fig.3, which well explains the amplitude changes of the 2AT-SMC control law u from an initial maximum to a smaller one shown in Fig.6(c). Then corresponding to phase 2 in Fig.3, as the system states tend to be stable, the amplitude of 2AT-SMC control law u remains adaptively variations in a sufficiently small range before PWM with the checking of the zero-crossing process of s. But for 2T-SMC, its control law u has obvious chattering due to the fixed control gain in Fig.6(c).

In particular, the output voltage v_c under discontinuous control law u of 1-SMC has an obvious chattering phenomenon, even if PWM is adopted to adjust the convergence boundary layer of s to mitigate the chattering, it still fails to achieve the desired effect [62]. But the 2-SM suppresses chattering well in Figure 6(a), (c), and (d).

Further, in Fig.6(d), three different zero-crossing reference numbers of N^* in (37) are selected for the comparison of the influence on the steady-state error of the system output in the zero-crossing detection mechanism when the controller gain changes over time. And the corresponding steady-state errors of v_c are 48.01mV, 6.23mV, and 3.01mV respectively. According to the selection formula of $N^* = \max\{2Tf_i + 1\}$, it concludes that the larger N^* is, the faster the frequency of the zero-crossing detection is, and the better performance of the adaptive variable gain control in the proposed 2AT-SMC method is. And the comparison results of N^* in Fig.6(d) also prove the positive effect of the online zero-crossing detection adaptive mechanism on the system performance. Therefore,

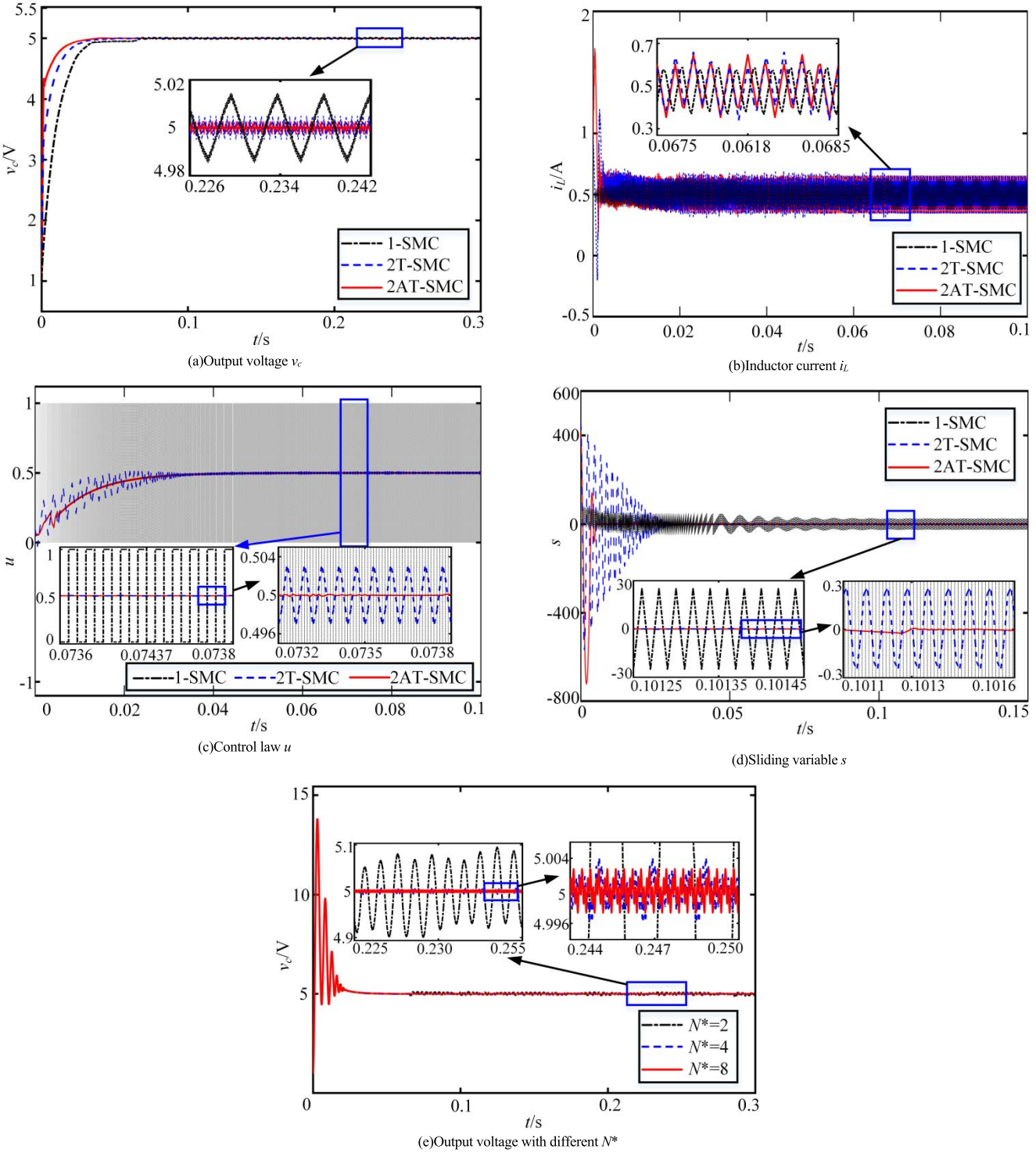

FIGURE 6. Comparative simulations in rated working condition.

we can select the appropriate positive parameters q_1 and q_2 related to the T in (39), then the N^* can be further determined for being compared with the calculated zero-crossings in (37), finally, the controller gain can be adjusted more precisely to balance the steady-state error of the system. Combining the selection of the N^* with the range of the sliding variable s and $\dot{s}$ in (40) and (41), we will see that the N^* affects the deviation range undergone by s and $\dot{s}$ by affecting the controller gain U_i in (37), i.e., the maximal deviation of the stability range of the system can be balanced effectively by selecting appropriate

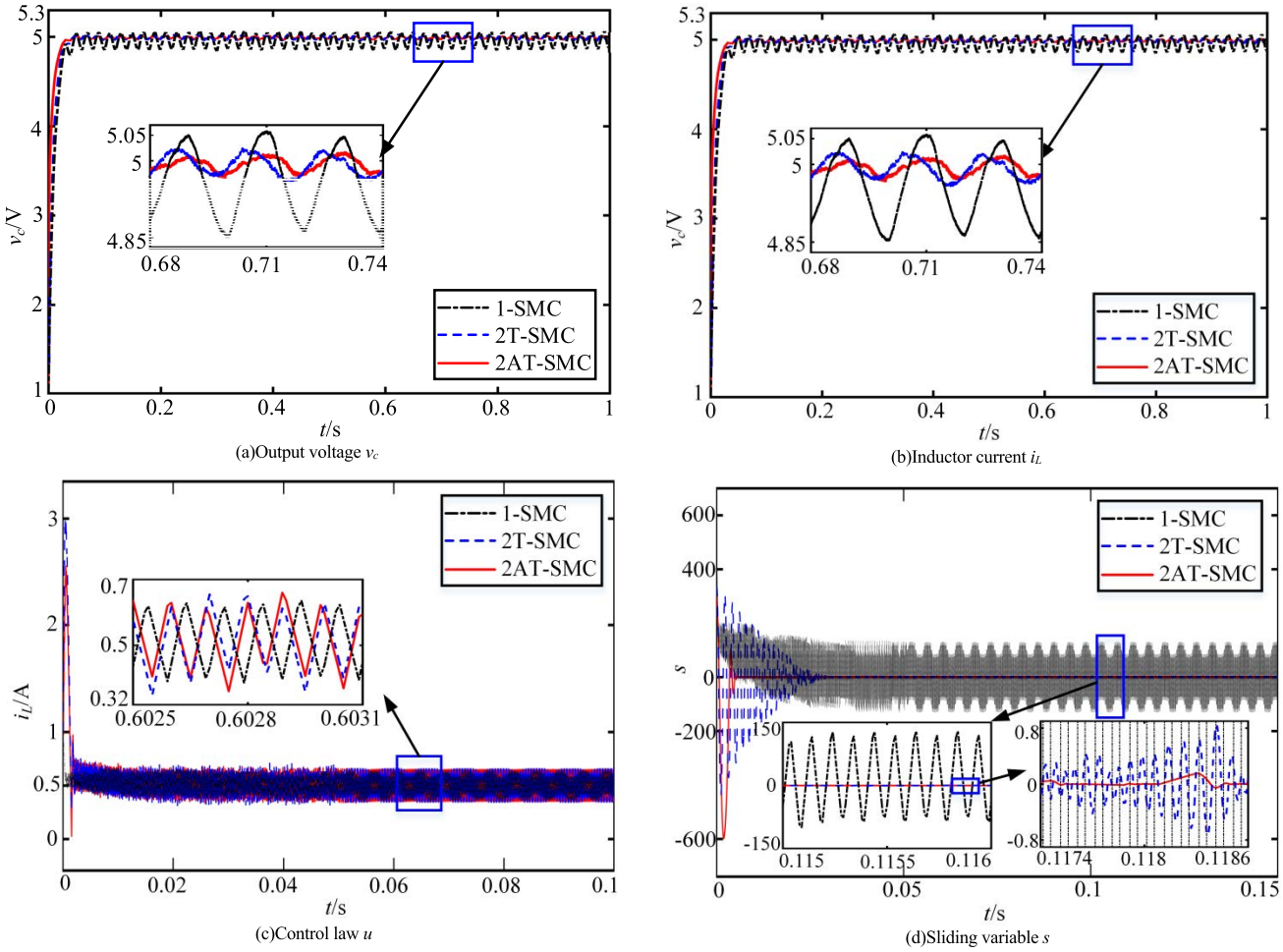

FIGURE 7. **Comparative simulations in multiple disturbances working condition.**

parameters T and N^*. By reducing the control magnitude at the minimum admissible level in the optimal deviation range of the system, the smaller region of the system output voltage can be further obtained.

Case 2: The working condition with multi-disturbances.

The equations (6)-(10) give the dynamic equation of the buck system with multi-disturbances. Combined with the analysis of practical application scenarios, the parameter disturbances of the system itself are considered as follows: the main parameters of the buck converter system are mainly disturbed by the external environment, such as DC voltage source E and reference voltage V_{ref}. But for the other parameters, their characteristics will lead to more than this. For the load resistor R, its value fluctuates within a certain range due to the change of its temperature during working; for the inductor L, due to the changes of its verified parasitic parameters and the resistance and core loss, its inductance value will change in the actual working process; For the capacitor C, which also has its own parasitic parameters, resulting in uncertain changes in its capacitance value as working [63]. Further, considering that the buck converter in working will be disturbed by the 50Hz AC power supply in the surrounding environment, and according to the general system, the disturbance range of each parameter does not exceed 10% of its own nominal value, the disturbance model of the above parameters is uniformly set as sine function form in the simulations in this paper, where the amplitude is 10% of their respective nominal values, and the frequency is 50Hz. The time-varying external disturbances $d_1(t)$ and $d_2(t)$ are mainly represented by noise interference in the working environment of the buck converter. And the specific forms of all disturbance sources are shown in Table 3 below.

The simulations considering multiple disturbances show the control performance comparisons of the buck system under the above three methods in Figure 7 and Table 4.

Comparing the rated working condition in Fig.6 and the multi-disturbances working condition in Fig.7, we can see the robustness of the SMC methods on the output voltage v_c, inductance current i_L, and control law u of the buck converter. Specifically, from Fig.7(a) and Table 4, it can be easily seen that the speed of system dynamic response to disturbances of 2AT-SMC is the fastest, and it recovers

TABLE 3. Internal and external disturbance signals of the buck system.

Disturbance Source	Disturbance Modle
ΔL	$0.1\sin(100\pi t)$(mH)
ΔC	$100\sin(100\pi t)$(μF)
ΔR	$\sin(100\pi t)$(Ω)
ΔE	$\sin(100\pi t)$(V)
ΔV_{ref}	$0.5\sin(100\pi t)$(V)
$d_1(t)$	$0.04\sin(4\times10^7\pi t)$(V)
$d_2(t)$	$0.04\sin(4\times10^7\pi t)$(V)

TABLE 4. Comparison of voltage and current in multi-disturbed working case.

SMC Algorithm	Output Voltage v_c		Inductor Current i_L	
	Steady-State Error(V)	Converge-nce Time(s)	Steady-State Error(A)	Converge-nce Time(s)
1-SMC	0.155	0.069	0.121	0.071
2T-SMC	0.051	0.050	0.233	0.057
2AT-SMC	0.025	0.039	0.135	0.040

to the steady-state at about 0.039s after adapting to all the disturbances, which can be attributed to the introduction of the zero-crossing detection mechanism shown Figure 3 for adjusting the controller gain continuously according to the time-varying disturbances. However, the convergence time of 2T-SMC and 1-SMC methods is only 0.050s and 0.069s respectively. And the v_c under the control of 2AT-SMC had the smallest fluctuation, only 0.025V, while for the 2T-SMC, its oscillation was larger with 0.051V, which can be due to the conventional 2-SM method using fixed gain. The comparison of control law u in Fig.7(c) and (d) can also explain the cause of v_c oscillation, i.e., under the multi-disturbances working condition, the control gain of the 2AT-SMC can change adaptively with the convergence process of zero-crossing detection mechanism of s under multi-disturbances and remain stable, while the conventional 2T-SMC with fixed gain cannot effectively drive the system states to be stable, every time the system suffering disturbances, the sliding variable s will vibrate strongly in Fig.7(d), so that the output voltage v_c oscillates greatly in the process of rapid convergence in Fig.7(a). In particular, the discontinuity control law u of 1-SMC in Fig.7(c) leads the large chattering of the sliding variable s about 140 in Fig.7(d), further weakening the ability of 1-SM to suppress the chattering of v_c compared with the 2-SM in Figure 7(a).

B. EXPERIMENTAL VERIFICATION

In order to validate the correctness of this paper, Figure 8 describes the structure of the experiment platform based on DSpace for the buck converter. The Rapid Control Prototype (RCP) system is composed of two parts, i.e.,

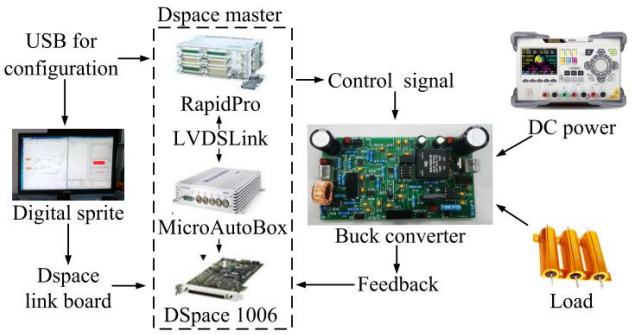

FIGURE 8. Structure diagram of the DSpace experimental system.

MicroAutoBox is used for collecting the output voltage v_c and inductance current i_L of the buck converter and RapidPro outputs the PWM signal for the direct control of the buck converter. Besides, they are linked with the interface of Low-Voltage Differential Signaling (LVDS). The software of Matlab/Simulink is installed on the host PC for developing algorithms following the program compiled by the Real-Time Work (RTW) shop and then downloaded in MicroAutoBox. The real-time calculation is in DSpace 1006.

In the experiment, the actual component parameters of the buck converter can refer to Table 1, and the controller parameters refer to the above simulation experiments. Further, in the specific operation, considering that the values of inductance L and capacitor C are reasonably disturbed due to the influence of their own parasitic parameters and external disturbance environment during actual working, therefore no additional disturbance signal is added to them. It can still be considered that $0 < \Delta L < 0.1$mH and $0 < \Delta C < 10^{-4}$F. For the disturbance simulations of other parameters, do the following operations: when the buck converter works stably under each SMC algorithm, the reference voltage V_{ref} changes from 5V to 5.5V at t_1, then the input voltage source E changes from 10V to 11V at t_2, and the resistance value of the load resistor R will change from 10Ω to 12Ω at t_3, i.e., the ΔV_{ref}, ΔE and ΔR are 0.5V, 1V and 2Ω, respectively. After the corresponding output signals of the system are observed, the disturbances of R, E, and V_{ref} will be removed successively at t_4, t_5, and t_6 respectively, so that the buck converter can return to the rated working condition. And the comparative experimental results of the three SMC algorithms are shown in Figure 9, wherein the 1s to 6s correspond to the moments t_1 to t_6, respectively.

The experimental results in Figure 9(a)-(b) verify the robust control effect of SMC on the buck converter under multi-disturbances conditions. In Fig.9(a), under the rated working condition of 0-t_1, the steady-state error of v_c output by 2AT-SMC is the smallest, only 0.15V, followed by 2T-SMC, which is 0.18V, while 1-SMC only is 0.37V. When the system is continuously disturbed by ΔV_{ref} and ΔE between t_1-t_3, the adaptive mechanism based on zero-crossing detection determines 2AT-SMC could ensure

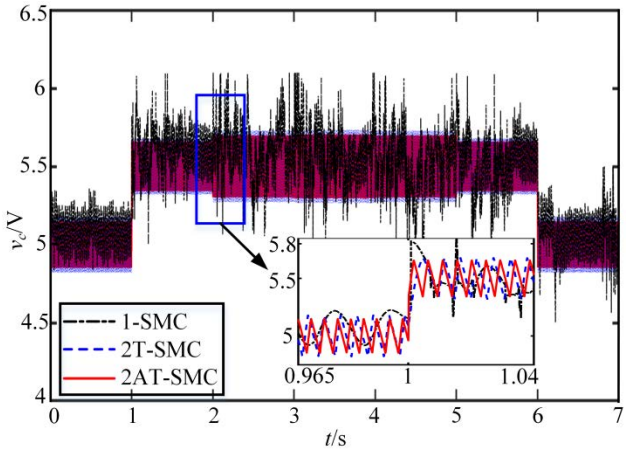

(a)Output voltage v_c

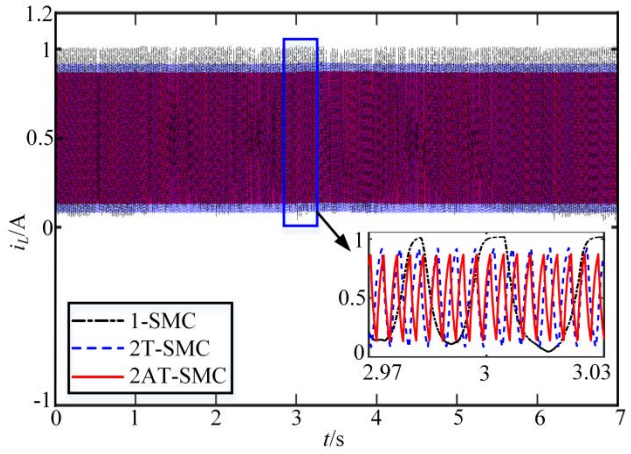

(b)Inductor current i_L

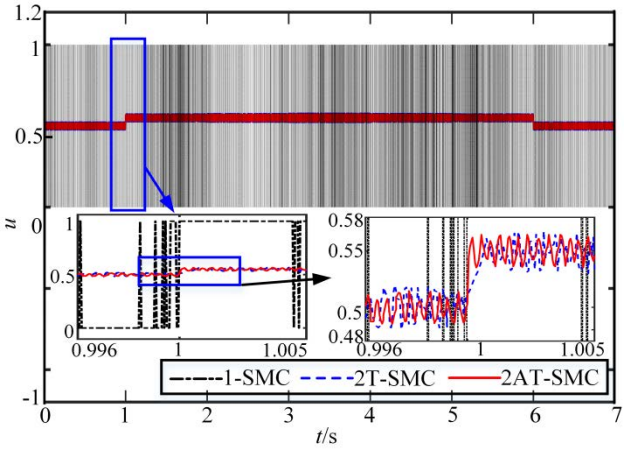

(c)Control law u

FIGURE 9. **Comparative experimental results in multiple disturbances working condition.**

the fastest dynamic response speed of the system, and ensure the minimum fluctuation range of v_c. And in Fig.9(a), the average response time of 2AT-SMC while suffering each disturbance is 0.084s, the 2T-SMC is 0.104s, and the 1-SMC is 0.126s. Between t_3-t_4, with the additional disturbance of ΔR, the system is in the condition of multi-disturbances. By contrast, 2AT-SMC can still ensure the smallest steady-error of the system within the range of 0.15V due to the magnitude of control law u that can be adaptively adjusted online in Fig.9(c), And 2T-SMC can only maintain the steady-error of the system within 0.185V due to the limitation of fixed gain in Fig.9(c). The adaptive control characteristics of 2AT-SMC to the system show the steady-state error of i_L in Fig.9(b) with 0.37A, while the 2T-SMC and 1-SMC are 0.42V and 0.5V respectively. The 1-SMC has a large voltage spike whenever the system is disturbed due to the discontinuous switching term sgn(·) in its control law in Fig.9(c).

Based on the performance comparison of buck converter under rated and multiple disturbance conditions from two aspects of simulations and experiments, the advantages of 2AT-SMC based on the adaptive mechanism of online zero-crossing detection proposed in this paper in chattering suppression, response speed, and control accuracy have been proved. It also shows that 2AT-SMC does improve the output voltage quality of the converter.

VI. CONCLUSION

This paper proposes a unified approach to modeling within buck converters for multiple model uncertainties and external disturbances. Most importantly, an improved adaptive twisting algorithm is proposed for buck converters on the basis of zero-crossing mechanism, which can further guarantee the control continuity and robustness. Furthermore, by adding an integral term in the sliding mode surface to ensure the system's better output accuracy and control performance, and the control magnitude at the minimum admissible level can be provided by selecting a suitable reference number of zero-crossings N^*, then the small output range of the system can be further obtained. The robust stability problem of the proposed method is investigated and proved. Finally, the simulations and experiments validate the effectiveness for wider applications. For future work, The parameter optimization of the adaptive continuous SM controller based on zero-crossing detection can be further studied. And the parameter fluctuations of the buck converters under multi-disturbances can be further observed by some means to enhance the control performance of our adaptive method.

REFERENCES

[1] Y. Wang, Z. Niu, M. Yang, L. Sun, and W. Zhang, "Stability of sliding mode controlled buck converters with unmodelled dynamics of circuit elements and Hall sensor," *IET Power Electron.*, vol. 14, no. 3, pp. 602–613, Feb. 2021.

[2] C. Wang, H. Xia, Y. Wang, and S. Ren, "A novel adaptive-gain higher-order sliding mode controller and its parameters tuning," *Nonlinear Dyn.*, vol. 107, no. 1, pp. 1049–1062, Jan. 2022.

[3] S.-C. Tan, Y. M. Lai, M. K. H. Cheung, and C. K. Tse, "On the practical design of a sliding mode voltage controlled buck converter," *IEEE Trans. Power Electron.*, vol. 20, no. 2, pp. 425–437, Mar. 2005.

[4] S. Ahmad and A. Ali, "Active disturbance rejection control of DC–DC boost converter: A review with modifications for improved performance," *IET Power Electron.*, vol. 12, no. 8, pp. 2095–2107, Jul. 2019.

[5] S.-C. Tan, Y. M. Lai, and C. K. Tse, "General design issues of sliding-mode controllers in DC–DC converters," *IEEE Trans. Ind. Electron.*, vol. 55, no. 3, pp. 1160–1174, Mar. 2008.

[6] H. Sira-Ramirez and M. A. Oliver-Salazar, "On the robust control of buck-converter DC-motor combinations," *IEEE Trans. Power Electron.*, vol. 28, no. 8, pp. 3912–3922, Aug. 2013.
[7] J. Yang, H. Cui, S. Li, and A. Zolotas, "Optimized active disturbance rejection control for DC–DC buck converters with uncertainties using a reduced-order GPI observer," *IEEE Trans. Circuits Syst. I, Reg. Papers*, vol. 65, no. 2, pp. 832–841, Feb. 2018.
[8] T. Guo, S. Huang, and X. Wang, "Overcurrent protection control design for DC–DC buck converter with disturbances," *IEEE Access*, vol. 7, pp. 90825–90833, 2019.
[9] X. Zhuang, Q. Zhang, Y. Liu, P. Zhu, X. Zheng, Y. Zeng, H. Guo, and Z. Zhang, "Phase shaping method for negative input admittance of buck converter based on sliding mode disturbance observer," *IEEE Access*, vol. 9, pp. 18287–18297, 2021.
[10] J. Linares-Flores, J. A. Juarez-Abad, A. Hernandez-Mendez, O. Castro-Heredia, J. F. Guerrero-Castellanos, R. Heredia-Barba, and G. Curiel-Olivares, "Sliding mode control based on linear extended state observer for DC-to-DC buck–boost power converter system with mismatched disturbances," *IEEE Trans. Ind. Appl.*, vol. 58, no. 1, pp. 940–950, Jan. 2022.
[11] J. Lu, M. Savaghebi, Y. Guan, J. C. Vasquez, A. M. Y. M. Ghias, and J. M. Guerrero, "A reduced-order enhanced state observer control of DC–DC buck converter," *IEEE Access*, vol. 6, pp. 56184–56191, 2018.
[12] K. Lakomy, R. Madonski, B. Dai, J. Yang, P. Kicki, M. Ansari, and S. Li, "Active disturbance rejection control design with suppression of sensor noise effects in application to DC–DC buck power converter," *IEEE Trans. Ind. Electron.*, vol. 69, no. 1, pp. 816–824, Jan. 2022.
[13] Y. Yin, J. Liu, A. Marquez, X. Lin, J. I. Leon, S. Vazquez, L. G. Franquelo, and L. Wu, "Advanced control strategies for DC–DC buck converters with parametric uncertainties via experimental evaluation," *IEEE Trans. Circuits Syst. I, Reg. Papers*, vol. 67, no. 12, pp. 5257–5267, Dec. 2020.
[14] J. Yang, W. X. Zheng, S. Li, and B. Wu, "Design of a prediction-accuracy-enhanced continuous-time MPC for disturbed systems via a disturbance observer," *IEEE Trans. Ind. Electron.*, vol. 62, no. 9, pp. 5807–5816, Sep. 2015.
[15] J. Sun, J. Yang, W. X. Zheng, and S. Li, "GPIO-based robust control of nonlinear uncertain systems under time-varying disturbance with application to DC–DC converter," *IEEE Trans. Circuits Syst. II, Exp. Briefs*, vol. 63, no. 11, pp. 1074–1078, Nov. 2016.
[16] G. Bartolini, E. Punta, and T. Zolezzi, "Approximability properties for second-order sliding mode control systems," *IEEE Trans. Autom. Control*, vol. 52, no. 10, pp. 1813–1825, Oct. 2007.
[17] S. S. D. Xu, C. C. Chen, and Z. L. Wu, "Study of nonsingular fast terminal sliding-mode fault-tolerant control," *IEEE Trans. Ind. Electron.*, vol. 62, no. 6, pp. 3906–3913, Jun. 2015.
[18] G. P. Incremona, M. Rubagotti, and A. Ferrara, "Sliding mode control of constrained nonlinear systems," *IEEE Trans. Autom. Control*, vol. 62, no. 6, pp. 2965–2972, Jun. 2017.
[19] P. Mattavelli, L. Rossetto, G. Spiazzi, and P. Tenti, "General-purpose fuzzy controller for DC–DC converters," *IEEE Trans. Power Electron.*, vol. 12, no. 1, pp. 79–86, Jan. 1997.
[20] B. Babes, S. Mekhilef, A. Boutaghane, and L. Rahmani, "Fuzzy approximation-based fractional-order nonsingular terminal sliding mode controller for DC–DC buck converters," *IEEE Trans. Power Electron.*, vol. 37, no. 3, pp. 2749–2760, Mar. 2022.
[21] A. Rubaai, A. R. Ofoli, L. Burge, and M. Garuba, "Hardware implementation of an adaptive network-based fuzzy controller for DC–DC converters," *IEEE Trans. Ind. Appl.*, vol. 41, no. 6, pp. 1557–1565, Nov. 2005.
[22] G. Rojas-Duenas, J.-R. Riba, and M. Moreno-Eguilaz, "Black-box modeling of DC–DC converters based on wavelet convolutional neural networks," *IEEE Trans. Instrum. Meas.*, vol. 70, pp. 1–9, 2021.
[23] R. F. Bastos, C. R. Aguiar, A. F. Q. Goncalves, and R. Q. Machado, "An intelligent control system used to improve energy production from alternative sources with DC/DC integration," *IEEE Trans. Smart Grid*, vol. 5, no. 5, pp. 2486–2495, Sep. 2014.
[24] M. H. Khooban, M. Gheisarnejad, H. Farsizadeh, A. Masoudian, and J. Boudjadar, "A new intelligent hybrid control approach for DC–DC converters in zero-emission ferry ships," *IEEE Trans. Power Electron.*, vol. 35, no. 6, pp. 5832–5841, Jun. 2020.
[25] J. Hu, H. Zhang, H. Liu, and X. Yu, "A survey on sliding mode control for networked control systems," *Int. J. Syst. Sci.*, vol. 52, no. 6, pp. 1129–1147, Apr. 2021.
[26] A. R. Gautam, K. Gourav, J. M. Guerrero, and D. M. Fulwani, "Ripple mitigation with improved line-load transients response in a two-stage DC–DC–AC converter: Adaptive SMC approach," *IEEE Trans. Ind. Electron.*, vol. 65, no. 4, pp. 3125–3135, Apr. 2018.
[27] S. Fan, X. Xiang, J. Sheng, Y. Gu, H. Yang, W. Li, X. He, and T. C. Green, "Inherent SM voltage balance for multilevel circulant modulation in modular multilevel DC–DC converters," *IEEE Trans. Power Electron.*, vol. 37, no. 2, pp. 1352–1368, Feb. 2022.
[28] Y. Wang, P. Huang, S. Ji, and M. Dai, "Improved linear sliding mode controller of buck converters through adding terminal sliding mode," in *Proc. 11th Asian Control Conf. (ASCC)*, Dec. 2017, pp. 682–686.
[29] A. Mohammadpour Shotorbani and E. Babaei, "Robust nonlinear controller based on control Lyapunov function and terminal sliding mode for buck converter," *Int. J. Numer. Modelling: Electron. Netw., Devices Fields*, vol. 29, no. 6, pp. 1055–1069, Nov. 2016.
[30] H. Komurcugil, "Non-singular terminal sliding-mode control of DC–DC buck converters," *Control Eng. Pract.*, vol. 21, no. 3, pp. 321–332, Mar. 2013.
[31] J. Wang, S. Li, J. Yang, B. Wu, and Q. Li, "Extended state observer-based sliding mode control for PWM-based DC–DC buck power converter systems with mismatched disturbances," *IET Control Theory Appl.*, vol. 9, no. 4, pp. 579–586, Feb. 2015.
[32] Z. Wang, S. Li, and Q. Li, "Continuous nonsingular terminal sliding mode control of DC–DC boost converters subject to time-varying disturbances," *IEEE Trans. Circuits Syst. II, Exp. Briefs*, vol. 67, no. 11, pp. 2552–2556, Nov. 2020.
[33] B. Xu, L. Zhang, and W. Ji, "Improved non-singular fast terminal sliding mode control with disturbance observer for PMSM drives," *IEEE Trans. Transport. Electrific.*, vol. 7, no. 4, pp. 2753–2762, Dec. 2021.
[34] A. Eltayeb, M. F. Rahmat, M. A. M. Basri, M. A. M. Eltoum, and S. El-Ferik, "An improved design of an adaptive sliding mode controller for chattering attenuation and trajectory tracking of the quadcopter UAV," *IEEE Access*, vol. 8, pp. 205968–205979, 2020.
[35] B.-Z. Guo, H.-C. Zhou, A. S. AL-Fhaid, A. M. M. Younas, and A. Asiri, "Stabilization of Euler-Bernoulli beam equation with boundary moment control and disturbance by active disturbance rejection control and sliding mode control approaches," *J. Dyn. Control Syst.*, vol. 20, no. 4, pp. 539–558, Oct. 2014.
[36] I. Boiko and L. Fridman, "Analysis of chattering in continuous sliding-mode controllers," *IEEE Trans. Autom. Control*, vol. 50, no. 9, pp. 1442–1446, Sep. 2005.
[37] A. Rosales, Y. Shtessel, L. Fridman, and C. B. Panathula, "Chattering analysis of HOSM controlled systems: Frequency domain approach," *IEEE Trans. Autom. Control*, vol. 62, no. 8, pp. 4109–4115, Aug. 2017.
[38] W. Gao and J. C. Hung, "Variable structure control of nonlinear systems: A new approach," *IEEE Trans. Ind. Electron.*, vol. 40, no. 1, pp. 45–55, Feb. 1993.
[39] J. J. Slotine and S. S. Sastry, "Tracking control of non-linear systems using sliding surfaces with application to robot manipulators," in *Proc. Amer. Control Conf.*, Jun. 1983, pp. 132–135.
[40] R. Palm, "Sliding mode fuzzy control," in *Proc. IEEE Int. Conf. Fuzzy Syst.*, Mar. 1992, pp. 519–526.
[41] A. Levant, "Principles of 2-sliding mode design," *Automatica*, vol. 43, no. 4, pp. 576–586, 2007.
[42] Y. B. Shtessel, S. Baev, C. Edwards, and S. Spurgeon, "HOSM observer for a class of non-minimum phase causal nonlinear MIMO systems," *IEEE Trans. Autom. Control*, vol. 55, no. 2, pp. 543–548, Feb. 2010.
[43] S. M. RakhtAla, M. Yasoubi, and H. HosseinNia, "Design of second order sliding mode and sliding mode algorithms: A practical insight to DC–DC buck converter," *IEEE/CAA J. Autom. Sinica*, vol. 4, no. 3, pp. 483–497, Jul. 2017.
[44] M. Lazar, W. P. M. H. Heemels, B. J. P. Roset, H. Nijmeijer, and P. P. J. van den Bosch, "Input-to-state stabilizing sub-optimal NMPC with an application to DC–DC converters," *Int. J. Robust Nonlinear Control*, vol. 18, no. 8, pp. 890–904, May 2008.
[45] S. M. Rakhtala and A. Casavola, "Real-time voltage control based on a cascaded super twisting algorithm structure for DC–DC converters," *IEEE Trans. Ind. Electron.*, vol. 69, no. 1, pp. 633–641, Jan. 2022.
[46] J. Yuan, S. Ding, and K. Mei, "Fixed-time SOSM controller design with output constraint," *Nonlinear Dyn.*, vol. 102, no. 3, pp. 1567–1583, 2020.
[47] L. Liu and S. Ding, "A unified control approach to finite-time stabilization of SOSM dynamics subject to an output constraint," *Appl. Math. Comput.*, vol. 394, Apr. 2021, Art. no. 125752.

[48] L. Liu, S. Ding, and X. Yu, "Second-Order sliding mode control design subject to an asymmetric output constraint," *IEEE Trans. Circuits Syst. II, Exp. Briefs*, vol. 68, no. 4, pp. 533–542, Apr. 2021.
[49] A. Farhoud and A. Erfanian, "Fully automatic control of paraplegic FES pedaling using higher-order sliding mode and fuzzy logic control," *IEEE Trans. Neural Syst. Rehabil. Eng.*, vol. 22, no. 3, pp. 533–542, May 2014.
[50] L. Djilali, A. Badillo-Olvera, Y. Yuliana Rios, H. Lopez-Beltran, and L. Saihi, "Neural high order sliding mode control for doubly fed induction generator based wind turbines," *IEEE Latin Amer. Trans.*, vol. 20, no. 2, pp. 223–232, Feb. 2022.
[51] G. V. Hollweg, P. J. D. de Oliveira Evald, D. M. C. Milbradt, R. V. Tambara, and H. A. Gründling, "Lyapunov stability analysis of discrete-time robust adaptive super-twisting sliding mode controller," *Int. J. Control*, vol. 2021, pp. 1–14, Dec. 2021.
[52] S. Mobayen, F. Bayat, C. C. Lai, A. Taheri, and A. Fekih, "Adaptive global sliding mode controller design for perturbed DC–DC buck converters," *Energies*, vol. 14, no. 5, pp. 1249–1261, Mar. 2021.
[53] M. Salimi and A. Zakipour, "Lyapunov based adaptive-robust control of the non-minimum phase DC–DC converters using input-output linearization," *J. Power Electron.*, vol. 15, no. 6, pp. 1577–1583, Nov. 2015.
[54] M. Salimi, "Practical implementation of the Lyapunov based nonlinear controller in DC–DC boost converter for MPPT of the PV systems," *Sol. Energy*, vol. 173, pp. 246–255, Oct. 2018.
[55] A. Pisano, M. Tanelli, and A. Ferrara, "Combined switched/time-based adaptation in second order sliding mode control," in *Proc. 52nd IEEE Conf. Decis. Control*, Dec. 2013, pp. 4272–4277.
[56] S. Maity, "Dynamics and stability issues of a discretized sliding-mode controlled DC–DC buck converter governed by fixed-event-time switching," *IEEE Trans. Circuits Syst. I, Reg. Papers*, vol. 60, no. 6, pp. 1657–1669, Jun. 2013.
[57] A. Pisano, M. Tanelli, and A. Ferrara, "Switched/time-based adaptation for second-order sliding mode control," *Automatica*, vol. 64, pp. 126–132, Feb. 2016.
[58] R. Garraoui, M. B. Hamed, and L. Sbita, "MPPT algorithms for PV system based on SM adaptive-FL and RCC method: A comparative study," in *Proc. 17th Int. Multi-Conf. Syst., Signals Devices (SSD)*, Jul. 2020, pp. 549–558.
[59] O. Kaplan and F. Bodur, "Second-order sliding mode controller design of buck converter with constant power load," *Int. J. Control*, vol. 2022, pp. 1–17, Feb. 2022.
[60] S. Hao, L. Hu, and P. X. Liu, "Second-order adaptive integral terminal sliding mode approach to tracking control of robotic manipulators," *IET Control Theory Appl.*, vol. 15, no. 17, pp. 2145–2157, Nov. 2021.
[61] Q. Zhang, R. Min, Q. Tong, X. Zou, Z. Liu, and A. Shen, "Sensorless predictive current controlled DC–DC converter with a self-correction differential current observer," *IEEE Trans. Ind. Electron.*, vol. 61, no. 12, pp. 6747–6757, Dec. 2014.
[62] W. Anjum, A. R. Husain, J. Abdul Aziz, M. A. Abbasi, and H. Alqaraghuli, "Continuous dynamic sliding mode control strategy of PWM based voltage source inverter under load variations," *PLoS ONE*, vol. 15, no. 2, Feb. 2020, Art. no. e0228636.
[63] M. Kumar and R. Gupta, "Stability and sensitivity analysis of uniformly sampled DC–DC converter with circuit parasitics," *IEEE Trans. Circuits Syst. I, Reg. Papers*, vol. 63, no. 11, pp. 2086–2097, Nov. 2016.

YANMIN WANG (Member, IEEE) received the B.Eng., M.Eng., and Ph.D. degrees in electrical engineering and automation from the Harbin Institute of Technology, Harbin, China, in 2002, 2005, and 2009, respectively.

From 2013 to 2014, she was a Visiting Scholar with the School of Computer Science and IT, RMIT University, Melbourne, VIC, Australia. Since 2017, she has been a member of the Green Energy Professional Committee of Chinese Architecture Society. In 2019, she has visited Monash University, Melbourne, supported by the Ministry of Industry and Information Technology, China, and the Harbin Institute of Technology. She is currently an Assistant Professor with the School of Electrical Engineering and Automation, Harbin Institute of Technology. Her research interests include sliding mode control, networked control, and building automation systems.

WEIQI ZHANG received the Bachelor of Building Electrical and Intelligent Engineering degree from the Harbin Institute of Technology, Harbin, China, where he is currently pursuing the master's degree in electrical engineering.

His research interests include sliding mode control and industrial automation systems.

CHEN XUE received the B.Eng. degree in automation from Shanghai University, Shanghai, China, in 2015, and the M.Eng. degree in mechanical engineering from the Harbin Institute of Technology, Harbin, China, in 2017, where he is currently pursuing the Ph.D. degree in electrical engineering.

He is also a Joint Ph.D. Student with the Center for Advanced Life Cycle Engineering (CALCE), University of Maryland, USA. His research interests include sliding mode control systems and battery management systems.